

Single-proton removal reaction in the IQMD+GEMINI model benchmarked by elemental fragmentation cross sections of $^{29-33}\text{Si}$ on carbon at ~ 230 MeV/nucleon

Guang-Shuai Li^a, Bao-Hua Sun^{a,*}, Jun Su^{b,*}, Isao Tanihata^{a,g}, Satoru Terashima^{c,a}, Jian-Wei Zhao^{d,e,a}, Er-Xi Xiao^b, Ji-Chao Zhang^a, Liu-Chun He^a, Ge Guo^a, Wei-Ping Lin^f, Wen-Jian Lin^a, Chuan-Ye Liu^a, Chen-Gui Lu^c, Bo Mei^{b,c}, Dan-Yang Pang^a, Ye-Lei Sun^a, Zhi-Yu Sun^c, Meng Wang^a, Feng Wang^a, Jing Wang^a, Shi-Tao Wang^c, Xiu-Lin Wei^a, Xiao-Dong Xu^{c,a}, Jun-Yao Xu^a, Li-Hua Zhu^a, Yong Zheng^c, Mei-Xue Zhang^a, Xue-Heng Zhang^c

^aSchool of Physics, Beihang University, Beijing 100191, China

^bSino-French Institute of Nuclear Engineering and Technology, Sun Yat-sen University, Zhuhai 519082, China

^cInstitute of Modern Physics, Chinese Academy of Sciences, Lanzhou 730000, China

^dState Key Laboratory of Nuclear Physics and Technology, School of Physics, Peking University, Beijing, 100871, China

^eGSI Helmholtzzentrum für Schwerionenforschung, D-64291, Darmstadt, Germany

^fKey Laboratory of Radiation Physics and Technology of the Ministry of Education, Institute of Nuclear Science and Technology, Sichuan University, Chengdu 610064, China

^gRCNP, Osaka University, Mihogaoka, Ibaraki, Osaka 567-0047, Japan

arXiv:2407.14697v1 [nucl-ex] 19 Jul 2024

Abstract

We report on the first measurement of the elemental fragmentation cross sections (EFCSs) of $^{29-33}\text{Si}$ on a carbon target at ~ 230 MeV/nucleon. The experimental data covering charge changes of $\Delta Z = 1-4$ are reproduced well by the isospin-dependent quantum molecular dynamics (IQMD) coupled with the evaporation GEMINI (IQMD+GEMINI) model. We further explore the mechanisms underlying the single-proton removal reaction in this model framework. We conclude that the cross sections from direct proton knockout exhibit a overall weak dependence on the mass number of Si projectiles. The proton evaporation induced after the projectile excitation significantly affects the cross sections for neutron-deficient Si isotopes, while neutron evaporation plays a crucial role in the reactions of neutron-rich Si isotopes. It is presented that the relative magnitude of one-proton and one-neutron separation energies is an essential factor that influences evaporation processes.

Keywords: elemental fragmentation cross sections, IQMD+GEMINI, single-proton removal reaction, proton evaporation

1. Introduction

The single-nucleon removal reaction is crucial for investigating the single-particle structure and nucleon-nucleon correlations within atomic nuclei [1]. Compilations of experimental nucleon removal cross sections for light projectile nuclei on composite targets (^9Be or ^{12}C) at intermediate energies have revealed that the reduction factor R_s strongly depends on the proton-neutron Fermi-surface asymmetry, which is quantified as $\Delta S = S_n - S_p$ for neutron removal or $\Delta S = S_p - S_n$ for proton removal [2–4], where S_p and S_n are the one-proton and one-neutron separation energies of a projectile, respectively. R_s is the ratio of experimental cross sections to theoretical predictions typically calculated using shell model spectroscopic factors and the eikonal reaction model that uses the adiabatic (or sudden) and eikonal approximations [5]. However, this dependence is inconsistent with the results from lower-energy transfer reactions [6, 7] and quasifree scattering involving ($p, 2p$), (p, pn), and ($e, e'p$) reactions at higher energies [8–10]. This inconsistency has persisted for nearly 20 years as a puzzle, attracting many attention from theoretical [11, 12] and experimental

studies [13–15]. For example, Hebborn *et al.* [16] showed that considering theoretical optical potential uncertainties in transfer and knockout reactions yields a consistent R_s - ΔS picture for loosely bound nucleons, while Rodríguez-Sánchez *et al.* [17] pointed out that incorporating short-range correlations (SRCs) into dynamic intranuclear cascade models could also eliminates the R_s - ΔS dependence for nucleon knockout reactions.

The inclusive single-nucleon removal cross section on a composite target at intermediate energies can involve contributions from different reaction mechanisms. The eikonal model has well-established diffraction breakup and stripping mechanisms at incident energies down to ~ 100 MeV/nucleon [18, 19], but it might not accurately describe the nucleon knockout process from deeply bound states. Moreover, non-direct reaction processes such as multiple scattering inside of the projectile and the excitation of the residues might influence the deeply bound nucleon-removal cross section on composite target. The eikonal model incorporates rescattering between projectile constituents only in an approximate way [20] and does not explicitly account for the evaporation channels in its calculation [21]. Additionally, valence-core destruction effects caused by interactions between the residual core and removed valence nucleon in nucleon knockout reactions are not included in the eikonal model [22].

*Corresponding Author

Email addresses: bhsun@buaa.edu.cn (Bao-Hua Sun),
sujun3@mail.sysu.edu.cn (Jun Su)

The single-nucleon removal reactions of ^9C and ^{13}O on ^9Be target at ~ 65 MeV/nucleon revealed that the proton evaporation components induced after projectile excitation account for roughly 17% and 21% of the cross sections, respectively [23]. Furthermore, in the $^{14}\text{O}(p, 2p)$ reaction at ~ 100 MeV/nucleon, the proton evaporation is evaluated to contribute nearly as much to the cross section as quasifree knockout [15]. Both experiments emphasize the significant role of proton evaporation in single-proton removal reactions. Although in Ref. [15] the proton is used as the target, the composite target is supposed to have a similar mechanism.

In this work, we aim to provide an alternative approach to understanding the mechanisms underlying single-proton removal reactions: the isospin-dependent quantum molecular dynamics (IQMD) model [24] together with the evaporation GEMINI model, *i.e.*, IQMD+GEMINI model. The IQMD model considers the evolution of nucleons in the mean-field potential and the nucleon-nucleon scatterings and thus includes the multiple scattering and excitation [25]. The GEMINI models the deexcitation of the highly excited pre-fragments [26]. Within this framework, one can assess how the projectile-like system's excitation and subsequent nucleon evaporation affect the elemental fragmentation cross sections (EFCs) and how the multiple reaction mechanisms contribute to the single-proton removal cross sections.

The IQMD+GEMINI model has been extensively employed in studying heavy-ion collisions at intermediate energies, particularly in reproducing the odd-even staggering effect in spallation and fragmentation reactions [27, 28]. To validate this model, we have measured the EFCs for fragments with charge changes of $\Delta Z = 1-4$ produced by $^{29-33}\text{Si}$ beams on a natural carbon target at ~ 230 MeV/nucleon. These measurements mark the first extension of EFCs to the neutron-rich Si isotopes. The newly obtained data, combined with the pioneering results for ^{28}Si fragments [29], are of significant importance for systematically exploring the patterns of fragment productions. Encouraged by promising results with the IQMD+GEMINI model, we then address the influence of multiple reaction mechanisms in single-proton removal reactions, such as direct knockout, multiple scattering, and nucleon evaporation [30] within the model framework.

2. Experiment

The EFCs of $^{29-33}\text{Si}$ nuclei on carbon were measured at the Heavy Ion Research Facility in Lanzhou (HIRFL) [31, 32]. A primary beam of 320 MeV/nucleon ^{40}Ar was impinged onto a 10 mm thick beryllium target positioned at the entrance of the Second Radioactive Ion Beam Line (RIBLL2) [33]. The resulting cocktail beams were transported to the External Target Facility (ETF). Nuclei $^{29-33}\text{Si}$ nuclei were identified on an event-by-event basis by a combination of magnetic rigidity ($B\rho$), energy deposition (ΔE), and time of flight (TOF) measurements. These nuclei were guided onto a natural carbon target with a thickness of 1.86 g/cm^2 .

A schematic layout of the experimental detector setup can be found in Ref. [29]. From the first dispersive focal plane (F1)

to ETF, the TOF resolution for the incoming beam was better than 80 ps [33–35]. A pair of multiple sampling ionization chambers (MUSICs) was positioned upstream and downstream of the reaction target to measure ΔE of incoming and outgoing particles. The large acceptance of MUSIC2, with an active area of $130 \text{ mm} \times 130 \text{ mm}$, guarantees the full coverage of outgoing heavy fragments. Both detectors had Z resolutions of 0.25-0.35 (FWHM) for ^{40}Ar products. The incident Si isotopes were separated using four different $B\rho$ settings, each optimized for the yield of $^{28,29}\text{Si}$, ^{30}Si , $^{31,32}\text{Si}$, and ^{33}Si . Furthermore, two plastic scintillators with a central hole were positioned upstream of the target to limit the position profile of incoming beams. Three multi-wire proportional chambers (MWPCs), two positioned upstream and one downstream of the reaction target, were used to determine the trajectories of incoming and outgoing particles. Positions from MWPC1 and MWPC2 were used to restrict the beam size at the target to $25 \text{ mm} \times 25 \text{ mm}$.

Measurements were also conducted without the reaction target to correct the effect of reactions in the materials other than the target (*e.g.*, detectors). The beam attenuation effect is taken into account for the precise EFCS determination for a thick target. Following the method in Ref. [29], the influence associated with the secondary reactions is evaluated to be negligibly small. Taking the target thickness into account, the EFCS for an incident beam with Z_i to an element with Z is calculated as

$$\sigma_{\Delta Z} = \left(\frac{N_F}{N_0} - \frac{N_F^O}{N_0^O} \right) \frac{\sigma_R}{1 - \exp(-\sigma_R t)}, \quad (1)$$

where the charge changes, $\Delta Z = Z_i - Z$, refer to the number of protons removed from the projectile. N_0 (N_0^O) and N_F (N_F^O) are the numbers of incident and outgoing particles for target-in (target-out) cases, respectively. The quantity t denotes the target thickness, and is expressed in the number of target nuclei per unit area. σ_R represents the reaction cross section of incident nuclei with the target nucleus, and is determined by the zero-range optical-limit Glauber model (ZRGm). The projectile's proton and neutron density distributions in this calculation are obtained from a Relativistic Hartree approach with density-dependent DD-ME2 parameter set [36] as inputs. A harmonic oscillator density distribution is employed for the ^{12}C target. An uncertainty of 5% in σ_R results in an error of about 0.3% in final EFCs.

Table 1 summarizes the EFCs measured in the present work for $^{29-33}\text{Si}$ nuclei on carbon at ~ 230 MeV/nucleon. The previous results for ^{28}Si from Ref. [29] are also included. For the EFCs with $\Delta Z = 1-4$, the statistical errors range from 4.9% to 11.4%. The systematic errors associated with the peak decoupling method are evaluated to be below 8.2%. Moreover, the secondary reactions in the target contribute to the systematic errors by about 2.5%, which are smaller than the statistical errors. The total errors of EFCs are estimated by adding the statistical and systematic errors in quadrature.

3. Theoretical approach

In the IQMD model, the many-body state is represented by a simple product wave function of single-particle states in a fixed

Table 1: Summary of elemental fragmentation cross sections (EFCs) for $^{29-33}\text{Si}$ nuclei on carbon at ~ 230 MeV/nucleon. The literature data taken from Ref. [29] for ^{28}Si are included. The error includes both statistical and systematic errors.

isotopes	Incident energy MeV/nucleon	$\sigma_{\Delta Z=1}$ mb	$\sigma_{\Delta Z=2}$ mb	$\sigma_{\Delta Z=3}$ mb	$\sigma_{\Delta Z=4}$ mb
^{33}Si	235	189 ± 17	131 ± 16	85 ± 10	96 ± 10^1
^{32}Si	232	208 ± 11	128 ± 9	87 ± 7	87 ± 7^1
^{31}Si	229	158 ± 13	125 ± 11	92 ± 10	79 ± 8^1
^{30}Si	225	170 ± 11	142 ± 10	83 ± 8	93 ± 7^1
^{29}Si	217	161 ± 11	144 ± 13	81 ± 11	89 ± 8^1
^{28}Si	218	140 ± 8	155 ± 9	91 ± 7	101 ± 9^2

¹ Present work.

² From Ref. [29].

Gaussian shape without anti-symmetrization

$$\psi(\mathbf{r}, t) = \prod_{i=1} \phi_i(\mathbf{r}, t), \quad (2)$$

$$\phi_i(\mathbf{r}, t) = \frac{1}{(2\pi L)^{3/4}} \exp\left[-\frac{[\mathbf{r} - \mathbf{r}_i(t)]^2}{4L}\right] \exp\left[\frac{i\mathbf{r} \cdot \mathbf{p}_i(t)}{\hbar}\right],$$

where \mathbf{r}_i and \mathbf{p}_i represent the average values of the positions and momenta of the i th nucleon. L is associated with the extension of the wave packet. The Wigner transform of the wave function derives the 1-body Wigner function. Then the density distribution function ρ of the system, which will be applied in the potential energy density functional, can be expressed as

$$\rho(\mathbf{r}) = \sum_i \frac{1}{(2\pi L)^{3/2}} \exp\left[-\frac{[\mathbf{r} - \mathbf{r}_i(t)]^2}{2L}\right]. \quad (3)$$

The Gaussian wave packets yield the following equations of motion derived from the time-dependent variational principle

$$\begin{aligned} \dot{\mathbf{r}}_i &= \nabla_{\mathbf{p}_i} H, \\ \dot{\mathbf{p}}_i &= -\nabla_{\mathbf{r}_i} H. \end{aligned} \quad (4)$$

Here, H represents the total N -body Hamiltonian, which consists of the kinetic energy, Coulomb potential energy, and local nuclear potential energy. The nuclear potential energy is a Skyrme-type integration of the potential energy density functional. The parameters are derived from the Skyrme parameters Sly6 [37] and provide a compressibility of 271 MeV at saturation density for isospin-symmetric nuclear matter. They are the same as those utilized in Ref. [29].

In addition to the mean-field propagation, the nucleon-nucleon scattering and the Pauli blocking effect of the final state are incorporated. The nucleon-nucleon scattering drives the stochastic evaluation and leads to enhanced fluctuations of the one-body density. Thus, in the philosophy of the IQMD model, one goes beyond the mean-field approach and includes correlations and fluctuations. The procedure of nucleon-nucleon scattering involves two steps: first, to determine if two test particles collide in a given time step, and second, to check whether the final state of the collision is allowed by the Pauli principle. Two nucleons collide in a given time step if they reach a distance of

the closest approach given by the cross section within that step. The choice of the final momenta of the nucleons is stochastic, with the condition that the total energy and momentum are conserved.

The calculation is a two-step process, including the dynamic evolution described by the IQMD and statistical decay by the GEMINI. The dynamic evolution time is selected as 100 fm/c. The GEMINI code receives inputs of atomic number, mass number, and excitation energy for each pre-fragment outputted by the IQMD model. If the excitation energy exceeds zero, the pre-fragment will decay by evaporating light particles (*e.g.*, n , p , α) and/or emitting γ rays. The particle decay widths are modeled using the Hauser-Feshbach formalism [38] for evaporation. For emitting a light particle (Z_1, A_1) with a spin of J_1 from a system (Z_0, A_0) with an excitation energy E^* and spin J_0 , resulting in the residual system (Z_2, A_2) with spin J_2 , the decay width Γ_{J_2} is given by

$$\begin{aligned} \Gamma_{J_2}(Z_1, A_1, Z_2, A_2) &= \frac{2J_1 + 1}{2\pi\rho_0} \sum_{l=|J_0-J_2|}^{J_0+J_2} \int_0^{E^*-B-E_{\text{rot}}} \\ &\times T_l(\varepsilon)\rho_2(E^* - B - E_{\text{rot}} - \varepsilon, J_2)d\varepsilon, \end{aligned} \quad (5)$$

where l and ε represent the orbital angular momentum and kinetic energy of the emitted particle, respectively. E_{rot} accounts for the rotational energy of the residual system. ρ_0 and ρ_2 denote the level densities of the initial and residual systems, respectively. The level densities follow the Fermi-gas prescription. [39]. The binding energy B is calculated from the nuclear masses. Nuclear masses and level densities with pairing correlations are adopted in the GEMINI model [27]. The tabulated masses are applied [40]. Detailed descriptions of the GEMINI model can be found in Ref. [26].

4. Results and discussion

Figures 1(a)–1(d) present the EFCs with $\Delta Z = 1-4$ fragments from $^{28-33}\text{Si}$ as a function of projectile mass number A . The experimental data from the present study are represented by black-filled circles, while the data from Ref. [29] are shown by open symbols. For $\Delta Z = 1$ residues, the EFCs tend to increase as the mass number increases. Similar trends of EFCs at $\Delta Z = 1$ are observed for Ca and Ti isotopes colliding with carbon at ~ 300 MeV/nucleon [41], as well as boron fragments produced from $^{12-16}\text{C}$ on carbon at ~ 240 MeV/nucleon [42]. Concerning the data at $\Delta Z = 2-4$, it is currently challenging to establish a definitive trend due to the relatively large uncertainties.

In Figs. 1(a)–1(d), the results of IQMD and IQMD+GEMINI model calculations are shown by the black dotted lines and by the red solid lines. One sees that the IQMD results exhibit a monotonically changing trend as ΔZ varies from 1 to 4 but fail to reproduce the experimental results. In contrast, the IQMD+GEMINI results reproduce the experimental data pretty well. This indicates the necessity of the statistical decay process beyond the dynamics in heavy-ion collisions [43, 44]. We also assessed predictions from the empirical parametrizations such as EPAX3 [45], modified EPAX2 [46], FRACS [47],

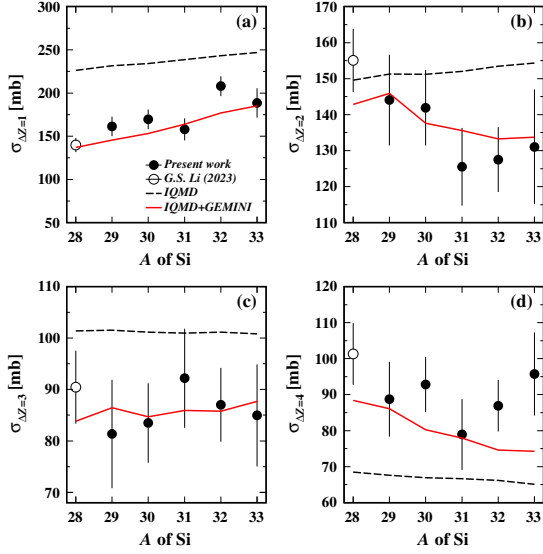


Figure 1: Elemental fragmentation cross sections (EFCs) for fragments with $\Delta Z = 1-4$, *i.e.*, (a) Al, (b) Mg, (c) Na, and (d) Ne isotopes, as a function of mass number A of $^{28-33}\text{Si}$ on carbon at ~ 230 MeV/nucleon. The present results are shown by filled circles, while the literature data taken from Ref. [29] are shown by open symbols. For comparison, the IQMD and the IQMD+GEMINI model predictions are shown as dashed and solid lines, respectively.

as well as the statistical models ABRABLA07 [48] and NUCFRG2 [49], but none of them predict the EFCs as effective as the IQMD+GEMINI model. Moreover, we find that the IQMD+GEMINI model can describe the other cross sections for different projectile-target combinations at various incident energies [29, 50–54]. Similar evidences of the significance of charged-particle evaporation were reported in the study of charge-changing reactions [55–57].

To study the dynamics leading to the projectile-like system excitation and sequential nucleon evaporation on EFCs, it is important to note the variation in the relationship between the IQMD and IQMD+GEMINI results. As seen in Figs. 1(a)-1(c), the IQMD+GEMINI model consistently predicts smaller cross sections for $\Delta Z = 1-3$ compared to those obtained from the IQMD model. The discrepancies between them decrease for larger ΔZ . Then, in contrast, the IQMD+GEMINI cross sections are larger than those of IQMD for $\Delta Z = 4$, as seen in Fig. 1(d). These observations can be explained by the higher excitation energy allowing for multiple sequential decay processes. Knocking out more protons will lead to more possible decay pathways. The decay path ending as a final fragment with higher stability will be chosen with a higher probability. Let the pre-fragment cross section to an element with Z in the IQMD model be σ_Z^{Pre} , then the fragment cross section σ_Z^{Fin} in the IQMD+GEMINI model can be written as $\sigma_Z^{\text{Fin}} = \sigma_Z^{\text{Pre}} - \sigma_{<Z}^{\text{evap}} + \sigma_{>Z}^{\text{evap}}$. Here $\sigma_{<Z}^{\text{evap}}$ represents the cross section that goes to lower- Z final fragments from pre-fragments with Z through the evaporation processes, which consequently reduces σ_Z^{Pre} . $\sigma_{>Z}^{\text{evap}}$ denotes the cross section from higher- Z pre-fragments that evaporate continuously to produce final residues with Z , leading to an increase of σ_Z^{Pre} . In Figs. 1(a)-1(d), σ_Z^{Pre} decreases rapidly with increasing ΔZ . This results in the reduc-

tion of $\sigma_{<Z}^{\text{evap}}$ since it constitutes a portion of σ_Z^{Pre} . In contrast, $\sigma_{>Z}^{\text{evap}}$ increases with ΔZ due to the increase in the number of pre-fragments. Consequently, the diversity of the decay pathways causes σ_Z^{Fin} to gradually approach σ_Z^{Pre} for $\Delta Z = 1-3$, but to surpass σ_Z^{Pre} for $\Delta Z = 4$. The shift in the relationship between the IQMD and the IQMD+GEMINI model calculations indicates the significance of the evaporation processes.

5. Single-proton removal in the IQMD+GEMINI model

The good agreement between the IQMD+GEMINI results and the experimental data allows for a detailed study of the underlying mechanisms of nucleon removal reactions. The IQMD+GEMINI model categorizes fragmentation into two distinct processes: hard nucleon collision and evaporation, which are treated by IQMD and GEMINI models, respectively. Under this framework, the emission of nucleon(s) together with the final residue can occur over different timescales. For the sake of clarity, we target the scenarios where only one proton is ejected from the ^{28}Si projectile as an example. Thus the reaction mechanisms for single-proton removal from ^{28}Si in collision with carbon to produce the final fragment ^{27}Al can be classified into three processes:

- (1) A proton is knocked out from initial ^{28}Si by a hard collision, leaving an excited pre-fragment $^{27}\text{Al}^*$. The pre-fragment $^{27}\text{Al}^*$ then decays via possible γ -ray emission and ends in the final residue ^{27}Al . This process is identified as the direct “proton knockout”.
- (2) The projectile-target collisions can also produce a pre-fragment having the identical mass and atomic number as initial ^{28}Si but in an excited state (*i.e.*, $^{28}\text{Si}^*$). Excited $^{28}\text{Si}^*$ then de-excites by evaporating a proton and possible γ -rays with ^{27}Al being the final fragment. This process is referred to as the “proton evaporation”. The strength of the evaporation is strongly correlated with the one-proton separation energy S_p .
- (3) The other processes, such as the “charge-exchange”, also contribute to the single-proton removal reaction. During the (p, n) charge-exchange, the excited $^{28}\text{Al}^*$ is initially produced in the hard collision stage and then de-excites by evaporating a neutron and possible γ -ray, resulting in the formation of ^{27}Al final fragment.

To evaluate the influences of those reaction mechanisms, we calculate the cross sections for proton knockout, proton evaporation, and charge-exchange processes that produce ^{A-1}Al fragments from the reactions of ^ASi ($A = 25-35$) with a carbon target at 230 MeV/nucleon using the IQMD+GEMINI model. As illustrated in Fig. 2(a), the charge-exchange cross sections typically amount to less than 6% of the total cross sections. The cross sections from the proton knockout depend weakly on the projectile mass number. This pattern significantly differs from the trend observed in the proton evaporation, where the cross sections decrease monotonically as the mass number increases up to $A = 29$ and then remain at very low values. This highlights

the significant influence of the proton evaporation on single-proton removal reactions for the neutron-deficient Si isotopes.

The trends in cross sections can be linked to the nucleon separation energies. Figure 2(b) presents the one-proton and one-neutron separation energies (S_p and S_n) of $^{25-35}\text{Si}$ nuclei. The S_p gradually increases with A , while S_n behaves in the opposite manner. Moreover, S_p is systematically smaller than S_n for $A \leq 28$, with the discrepancies being more pronounced toward the neutron-deficient side. This is exactly in accordance with the significant increase in cross sections for proton evaporation. Consequently, the projectile excitation followed by proton evaporation predominantly contributes to single-proton removal cross sections for $A \leq 28$.

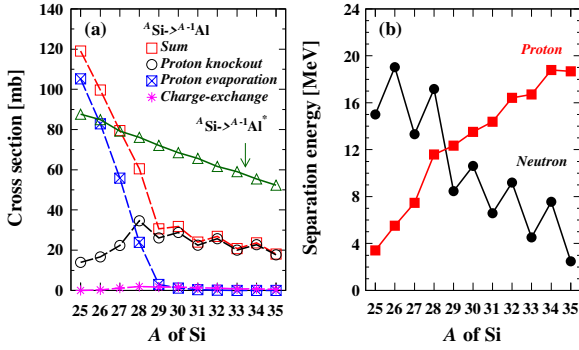


Figure 2: (a) The cross sections for proton knockout, proton evaporation, and charge-exchange processes, and their summation for ^{A-1}Al final fragments as a function of mass number A of Si ($A = 25-35$). For comparison, the cross sections of pre-fragments $^{A-1}\text{Al}^*$ are also shown by the open green triangles. (b) One-proton and one-neutron separation energies (S_p and S_n) of $^{25-35}\text{Si}$ nuclei are presented. Proton(neutron) evaporation predominantly influences single-proton removal reactions when $S_p(S_n)$ is less than $S_n(S_p)$. For the details, see the text.

As for $A \geq 29$, where S_p is consistently larger than S_n , the proton knockout plays a significant role in determining the cross sections rather than the proton evaporation. However, the proton knockout contributes much smaller cross sections for ^{A-1}Al fragments compared to those expected from the pre-fragments $^{A-1}\text{Al}^*$ generated by hard collisions, as shown in Fig. 2(a). The fragments ^{A-1}Al cross sections change almost in parallel with those of pre-fragments $^{A-1}\text{Al}^*$ for $A \geq 29$, where the contribution from the proton evaporation is negligibly small. About 60% of pre-fragments $^{A-1}\text{Al}^*$ cross sections are lost by evaporation. Considering the smaller S_n (or larger S_p) for the neutron-rich Si isotopes, it is believed that the neutron(s) evaporation from pre-fragments dominates and strongly reduces the pre-fragment cross sections. Moreover, the proton knockout cross sections typically decrease toward the neutron-deficient Si isotopes with $A \leq 28$. This is attributed to the increased contribution of proton evaporation from $^{A-1}\text{Al}^*$ pre-fragments to form lower- $(A - 1)$ final fragments, similar to the increase in proton evaporation cross sections from Si pre-fragments. The proton(neutron) evaporation becomes significant when the $S_p(S_n)$ is smaller than $S_n(S_p)$.

In Fig. 3, the EFCS results from the IQMD model for $\Delta Z = 1$ pre-fragments produced by $^{25-33}\text{Si}$ on carbon at 230 MeV/nucleon tend to increase as mass number A increases.

In contrast, the IQMD+GEMINI results exhibit a distinct kink at $A = 27$. This suggests that the proton evaporation predominantly influences fragment cross sections when A is less than 27, whereas neutron evaporation becomes increasingly significant for A greater than 27.

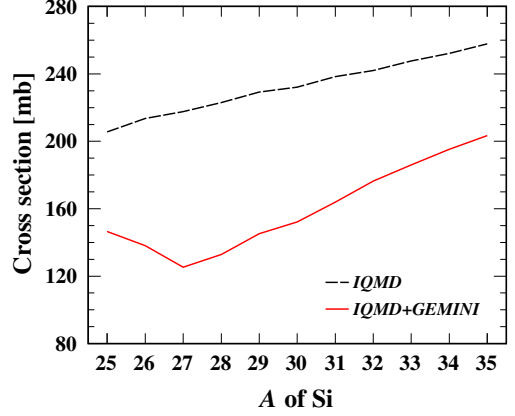


Figure 3: The EFCS results of $\Delta Z = 1$ pre-fragments (black line) and final fragments (red line) produced by $^{25-35}\text{Si}$ nuclei on carbon at 230 MeV/nucleon, which are simulated by using the IQMD and IQMD+GEMINI models, respectively.

The aforementioned discussion in Fig. 2(a) is supported by examining the fragment cross sections of different isotopes. Figure 4 presents such cross sections for ^{26}Si , ^{30}Si and ^{34}Si projectiles as examples. Both fragment (open symbols) and pre-fragment (filled symbols) cross sections are shown for comparison. In the fragmentation of ^{26}Si projectile, the cross section of fragment ^{25}Al is larger than that of pre-fragment $^{25}\text{Al}^*$. This indicates that the proton evaporation from excited $^{26}\text{Si}^*$ dominates the fragment cross section. The cross section of fragment ^{24}Al is much smaller than that of pre-fragment $^{24}\text{Al}^*$ and thus shows that the cross section is reduced by the evaporation process but is not much increased from neutron evaporation of heavier Al isotopes. A clear difference is seen in ^{34}Si projectile where fragment cross sections of Al isotopes with neutron removal are as large as those without neutron removal. In particular, the cross sections of fragments Al with mass number less than 29 are larger than those of pre-fragments, indicating the significant contribution from the neutron evaporation of heavier Al pre-fragments. Fragmentation of ^{30}Si clearly shows the transition from the neutron-deficient to the neutron-rich side of Al isotopes. Hence, neutron evaporation significantly influences the fragmentation of neutron-rich nuclei, whereas proton evaporation dominates the fragmentation of neutron-deficient nuclei.

6. Summary

We have presented the ETCSs of fragments with $\Delta Z = 1-4$ produced by $^{29-33}\text{Si}$ on a carbon target at ~ 230 MeV/nucleon. These measurements mark the first extension of EFCSs to the neutron-rich Si isotopes. The IQMD+GEMINI model reproduces the experimental data pretty well. Therefore, we explored the dynamics, the production of pre-fragments, and the

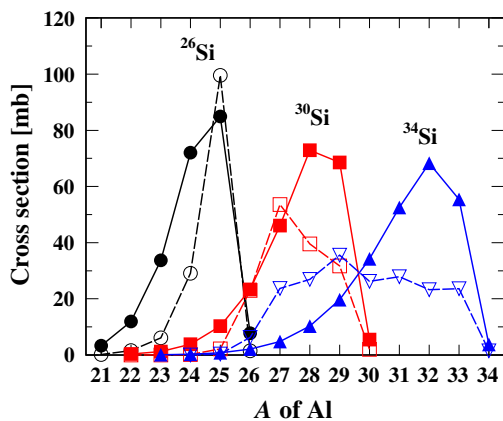


Figure 4: Fragment (open symbol) and pre-fragment (filled symbol) cross sections of Al isotopes produced by ^{26}Si , ^{30}Si and ^{34}Si projectiles colliding with carbon at 230 MeV/nucleon. The results from the fragmentation of these three projectiles are represented by black, red, and blue data points, respectively.

sequential nucleon evaporation by using the IQMD+GEMINI model. In particular, we studied the reaction mechanisms in single-proton removal reactions. We concluded that neutron evaporation from the pre-fragment strongly reduces the cross sections of neutron-rich nuclei, while proton evaporation from pre-fragment increases the cross sections of neutron-deficient nuclei. Currently, there is no experimental data available for neutron-deficient Si incident fragment cross sections. Such data would provide a crucial insights into our understanding of the evaporation processes. We showed that the IQMD+GEMINI model offers a new view of underlying mechanisms in single-proton removal reactions and other fragment reactions.

ACKNOWLEDGMENTS

The authors express their gratitude to the staff of the HIRFL-CSR accelerator for their dedicated efforts and assistance in maintaining a stable beam condition throughout the experiment. The authors are grateful to T. Yamaguchi for generously providing the experimental data in Ref. [41]. Special thanks are also due to Z. Z. Li and Y. F. Niu for their valuable contributions and assistance in determining the nucleon density distributions. This work was supported partially by the National Natural Science Foundation of China (Nos. 12325506, 11961141004, 11922501, 11475014, 11905260, the National Key R&D program of China (No. 2016YFA0400504). X. D. Xu acknowledges the support of the Western Light Project of the Chinese Academy of Sciences.

References

[1] T. Aumann, C. Barbieri, D. Bazin, C. Bertulani, A. Bonaccorso, W. Dickhoff, A. Gade, M. Gómez-Ramos, B. Kay, A. Moro, T. Nakamura, A. Obertelli, K. Ogata, S. Paschalis, T. Uesaka, *Quenching of single-particle strength from direct reactions with stable and rare-isotope beams*, *Prog. Part. Nucl. Phys.* 118 (2021) 103847. doi:<https://doi.org/10.1016/j.pnpnp.2021.103847>. URL <https://www.sciencedirect.com/science/article/pii/S0146641021000016>

[2] A. Gade, P. Adrich, D. Bazin, M. D. Bowen, B. A. Brown, C. M. Campbell, J. M. Cook, T. Glasmacher, P. G. Hansen, K. Hosier, S. McDaniel, D. McGlinchery, A. Obertelli, K. Siwek, L. A. Riley, J. A. Tostevin, D. Weisshaar, *Reduction of spectroscopic strength: Weakly-bound and strongly-bound single-particle states in ^{26}Si* , *Phys. Rev. C* 77 (2008) 044306. doi:[10.1103/PhysRevC.77.044306](https://doi.org/10.1103/PhysRevC.77.044306). URL <https://link.aps.org/doi/10.1103/PhysRevC.77.044306>

[3] J. A. Tostevin, A. Gade, *Systematics of intermediate-energy single-nucleon removal reactions in ^{26}Si* , *Phys. Rev. C* 90 (2014) 057602. doi:[10.1103/PhysRevC.90.057602](https://doi.org/10.1103/PhysRevC.90.057602). URL <https://link.aps.org/doi/10.1103/PhysRevC.90.057602>

[4] J. A. Tostevin, A. Gade, *Updated systematics of intermediate-energy single-nucleon removal reactions in ^{26}Si* , *Phys. Rev. C* 103 (2021) 054610. doi:[10.1103/PhysRevC.103.054610](https://doi.org/10.1103/PhysRevC.103.054610). URL <https://link.aps.org/doi/10.1103/PhysRevC.103.054610>

[5] P. Hansen, J. Tostevin, *Direct reactions with exotic nuclei*, *Annu. Rev. Nucl. Part. Sci.* 53 (2003) 219–261.

[6] J. Lee, M. B. Tsang, D. Bazin, D. Coupland, V. Henzl, D. Henzlova, M. Kilburn, W. G. Lynch, A. M. Rogers, A. Sanetullaev, A. Signoracci, Z. Y. Sun, M. Youngs, K. Y. Chae, R. J. Charity, H. K. Cheung, M. Famiano, S. Hudan, P. O’Malley, W. A. Peters, K. Schmitt, D. Shapira, L. G. Sobotka, *Neutron-proton asymmetry dependence of spectroscopic factors in ^{26}Si isotopes*, *Phys. Rev. Lett.* 104 (2010) 112701. doi:[10.1103/PhysRevLett.104.112701](https://doi.org/10.1103/PhysRevLett.104.112701). URL <https://link.aps.org/doi/10.1103/PhysRevLett.104.112701>

[7] F. Flavigny, A. Gillibert, L. Nalpas, A. Obertelli, N. Keeley, C. Barbieri, D. Beaumel, S. Boissinot, G. Burgunder, A. Cipollone, A. Corsi, J. Gibelin, S. Giron, J. Guillot, F. Hammache, V. Lapoux, A. Matta, E. C. Pollacco, R. Raabe, M. Rejmund, N. de Séville, A. Shrivastava, A. Signoracci, Y. Utsuno, *Limited asymmetry dependence of correlations from single nucleon transfer, ^{26}Si* , *Phys. Rev. Lett.* 110 (2013) 122503. doi:[10.1103/PhysRevLett.110.122503](https://doi.org/10.1103/PhysRevLett.110.122503). URL <https://link.aps.org/doi/10.1103/PhysRevLett.110.122503>

[8] M. Holl, V. Panin, H. Alvarez-Pol, L. Atar, T. Aumann, S. Beceiro-Novo, J. Benlliure, C. Bertulani, J. Boillos, K. Boretzky, M. Caamaño, C. Caesar, E. Casarejos, W. Catford, J. Cederkall, L. Chulkov, D. Cortina-Gil, E. Cravo, I. Dillmann, P. Díaz Fernández, Z. Elekes, J. Enders, L. Fraile, D. Galaviz Redondo, R. Gernhäuser, P. Golubev, T. Heftrich, M. Heil, M. Heine, A. Heinz, A. Henriques, H. Johansson, B. Jonson, N. Kalantar-Nayestanaki, R. Kanungo, A. Kelic-Heil, T. Kröll, N. Kurz, C. Langer, T. Le Bleis, S. Lindberg, J. Machado, E. Nacher, M. Najafi, T. Nilsson, C. Nociforo, S. Paschalis, M. Petri, R. Reifarh, G. Ribeiro, C. Rigollet, D. Rossi, D. Savran, H. Scheit, H. Simon, O. Sorlin, I. Syndikus, O. Tengblad, Y. Togano, M. Vandebrouck, P. Velho, F. Wamers, H. Weick, C. Wheldon, G. Wilson, J. Winfield, P. Woods, M. Zhukov, K. Zuber, *Quasi-free neutron and proton knockout reactions from light nuclei in a wide neutron energy range*, *Phys. Lett. B* 795 (2019) 682–688. doi:<https://doi.org/10.1016/j.physletb.2019.06.069>. URL <https://www.sciencedirect.com/science/article/pii/S03702693193037026931>

[9] M. Gómez-Ramos, A. Moro, *Binding-energy independence of reduced spectroscopic factors in ^{26}Si* , *Phys. Lett. B* 785 (2018) 511–516. doi:<https://doi.org/10.1016/j.physletb.2018.08.058>. URL <https://www.sciencedirect.com/science/article/pii/S03702693183037026931>

[10] C. Barbieri, L. Lapikás, *Effects of rescattering in $(e, e'p)$ reactions within a semiclassical approach*, *Phys. Rev. C* 70 (2004) 054612. doi:[10.1103/PhysRevC.70.054612](https://doi.org/10.1103/PhysRevC.70.054612). URL <https://link.aps.org/doi/10.1103/PhysRevC.70.054612>

[11] N. T. T. Phuc, K. Yoshida, K. Ogata, *Toward a reliable description of (p, pn) reactions in the distorted-wave impulse approximation*, *Phys. Rev. C* 100 (2019) 064604. doi:[10.1103/PhysRevC.100.064604](https://doi.org/10.1103/PhysRevC.100.064604). URL <https://link.aps.org/doi/10.1103/PhysRevC.100.064604>

[12] S. Paschalis, M. Petri, A. Macchiavelli, O. Hen, E. Piastetzky, *Nucleon-nucleon correlations and the single-particle strength in atomic nuclei, ^{26}Si* , *Phys. Lett. B* 800 (2020) 135110. doi:<https://doi.org/10.1016/j.physletb.2019.135110>. URL <https://www.sciencedirect.com/science/article/pii/S03702693193037026931>

[13] V. Panin, M. Holl, J. Taylor, Y. Aksyutina, H. Alvarez-Pol, T. Aumann, C. Bertulani, K. Boretzky, C. Caesar, M. Chartier, L. Chulkov, D. Cortina-Gil, J. Enders, O. Ershova, H. Geissel, R. Gernhäuser, M. Heil, H. Johansson, B. Jonson, A. Kelic-Heil, O. Kiselev, C. Langer, T. Le

- Bleis, R. Lemmon, T. Nilsson, S. Paschalis, M. Petri, R. Plag, R. Reifarth, D. Rossi, H. Scheit, H. Simon, F. Wamers, H. Weick, C. Wimmer, **Quasi-free proton knockout from ^{12}C on carbon target at 398 mev/u**, Phys. Lett. B 797 (2019) 134802. doi:<https://doi.org/10.1016/j.physletb.2019.134802>. URL <https://www.sciencedirect.com/science/article/pii/S0370269319305614>
- [14] J. Díaz-Cortés, J. Benlliure, J. Rodríguez-Sánchez, H. Álvarez Pol, T. Aumann, C. Bertulani, B. Blank, E. Casarejos, D. Cortina-Gil, D. Dragosavac, V. Föhr, A. Gargano, M. Gascón, W. Gawlikowicz, A. Heinz, K. Helariutta, A. Kelić-Heil, S. Lukić, F. Montes, D. Pérez-Loureiro, L. Pieńkowski, K.-H. Schmidt, M. Staniou, K. Subotić, K. Sümmerer, J. Taieb, A. Trzcińska, **Systematic reduction of the proton-removal cross section in neutron-rich medium-mass nuclei**, Phys. Lett. B 811 (2020) 135962. doi:<https://doi.org/10.1016/j.physletb.2020.135962>. URL <https://www.sciencedirect.com/science/article/pii/S0370269320307566>
- [15] T. Pohl, Y. L. Sun, A. Obertelli, J. Lee, M. Gómez-Ramos, K. Ogata, K. Yoshida, B. S. Cai, C. X. Yuan, B. A. Brown, H. Baba, D. Beaumel, A. Corsi, J. Gao, J. Gibelin, A. Gillibert, K. I. Hahn, T. Isobe, D. Kim, Y. Kondo, T. Kobayashi, Y. Kubota, P. Li, P. Liang, H. N. Liu, J. Liu, T. Lokotko, F. M. Marqués, Y. Matsuda, T. Motobayashi, T. Nakamura, N. A. Orr, H. Otsu, V. Panin, S. Y. Park, S. Sakaguchi, M. Sasano, H. Sato, H. Sakurai, Y. Shimizu, A. I. Stefanescu, L. Stuhl, D. Suzuki, Y. Togano, D. Tudor, T. Uesaka, H. Wang, X. Xu, Z. H. Yang, K. Yoneda, J. Zenihiro, **Multiple mechanisms in proton-induced nucleon removal at ~ 100 MeV/Nucleon**, Phys. Rev. Lett. 130 (2023) 172501. doi:<https://doi.org/10.1103/PhysRevLett.130.172501>. URL <https://link.aps.org/doi/10.1103/PhysRevLett.130.172501>
- [16] C. Hebborn, F. M. Nunes, A. E. Lovell, **New perspectives on spectroscopic factor quenching from reactions**, Phys. Rev. Lett. 131 (2023) 212503. doi:<https://doi.org/10.1103/PhysRevLett.131.212503>. URL <https://link.aps.org/doi/10.1103/PhysRevLett.131.212503>
- [17] J. Rodríguez-Sánchez, J. Cugnon, J. David, J. Hirtz, **Short-range correlations in dynamical intranuclear cascade models for describing nuclei**, Phys. Lett. B 851 (2024) 138559. doi:<https://doi.org/10.1016/j.physletb.2024.138559>. URL <https://www.sciencedirect.com/science/article/pii/S0370269324051175>
- [18] D. Bazin, R. J. Charity, R. T. de Souza, M. A. Famiano, A. Gade, V. Henzl, D. Henzlova, S. Hudan, J. Lee, S. Lukyanov, W. G. Lynch, S. McDaniel, M. Mocko, A. Obertelli, A. M. Rogers, L. G. Sobotka, J. R. Terry, J. A. Tostevin, M. B. Tsang, M. S. Wallace, **Mechanisms in knockout reactions**, Phys. Rev. Lett. 102 (2009) 232501. doi:<https://doi.org/10.1103/PhysRevLett.102.232501>. URL <https://link.aps.org/doi/10.1103/PhysRevLett.102.232501>
- [19] K. Wimmer, D. Bazin, A. Gade, J. A. Tostevin, T. Baugher, Z. Chajecski, D. Coupland, M. A. Famiano, T. K. Ghosh, G. F. Grinyer, M. E. Howard, M. Kilburn, W. G. Lynch, B. Manning, K. Meierbachtol, P. Quarterman, A. Ratkiewicz, A. Sanetullaev, R. H. Showalter, S. R. Stroberg, M. B. Tsang, D. Weisshaar, J. Winkelbauer, R. Winkler, M. Youngs, **Elastic breakup cross sections of well-bound nucleons**, Phys. Rev. C 90 (2014) 064615. doi:<https://doi.org/10.1103/PhysRevC.90.064615>. URL <https://link.aps.org/doi/10.1103/PhysRevC.90.064615>
- [20] R. Crespo, A. Deluva, E. Cravo, **Rescattering effects for the $^{12}\text{C}(p, 2p)^{11}\text{B}$ reaction at 400 mev/u**, Phys. Rev. C 90 (2014) 044606. doi:<https://doi.org/10.1103/PhysRevC.90.044606>. URL <https://link.aps.org/doi/10.1103/PhysRevC.90.044606>
- [21] Y. L. Sun, J. Lee, Y. L. Ye, A. Obertelli, Z. H. Li, N. Aoi, H. J. Ong, Y. Ayyad, C. A. Bertulani, J. Chen, A. Corsi, F. Cappuzzello, M. Cavallaro, T. Furono, Y. C. Ge, T. Hashimoto, E. Ideguchi, T. Kawabata, J. L. Lou, Q. T. Li, G. Lorusso, F. Lu, H. N. Liu, S. Nishimura, H. Suzuki, J. Tanaka, M. Tanaka, D. T. Tran, M. B. Tsang, J. Wu, Z. Y. Xu, T. Yamamoto, **Experimental study of the knockout reaction mechanism using ^{14}O at 60 mev/nucleon**, Phys. Rev. C 93 (2016) 044607. doi:<https://doi.org/10.1103/PhysRevC.93.044607>. URL <https://link.aps.org/doi/10.1103/PhysRevC.93.044607>
- [22] M. Gómez-Ramos, J. Gómez-Camacho, A. Moro, **Isospin dependence in single-nucleon removal cross sections explained through valence nucleon effects**, Phys. Lett. B 847 (2023) 138284. doi:<https://doi.org/10.1016/j.physletb.2023.138284>. URL <https://www.sciencedirect.com/science/article/pii/S0370269323006184>
- [23] R. J. Charity, L. G. Sobotka, J. A. Tostevin, **Single-nucleon knockout cross sections for reactions producing resonance states at 102 mev/u**, Phys. Rev. C 102 (2020) 044614. doi:<https://doi.org/10.1103/PhysRevC.102.044614>. URL <https://link.aps.org/doi/10.1103/PhysRevC.102.044614>
- [24] R. Charity, L. Zhuxia, L. Neise, G. Peilert, A. Rosenhauer, H. Sorge, J. Aichelin, H. Stöcker, W. Greiner, **Quantum molecular dynamics a microscopic model from unilac to cern energies**, Nucl. Phys. A 495 (1989) 303–319. doi:[https://doi.org/10.1016/0375-9474\(89\)90328-X](https://doi.org/10.1016/0375-9474(89)90328-X). URL <https://www.sciencedirect.com/science/article/pii/0375947489>
- [25] H. Wolter, M. Colonna, D. Cozma, P. Danielewicz, C. M. Ko, R. Kumanishi, M. B. Tsang, J. Xu, Y.-X. Zhang, E. Bratkovskaya, Z.-Q. Feng, T. Gaitanos, A. Le Fèvre, N. Ikeno, Y. Kim, S. Mallik, P. Napolitani, D. Oliinychenko, T. Ogawa, M. Papa, J. Su, R. Wang, J. Weil, F.-S. Zhang, G.-Q. Zhang, Z. Zhang, J. Aichelin, W. Cassing, L.-W. Chen, H.-G. Cheng, H. Elfner, K. Gallmeister, C. Hartnack, S. Hashimoto, S. Jeon, K. Kim, M. Kim, B.-A. Li, C.-H. Lee, Q.-F. Li, Z.-X. Li, U. Mosel, Y. Nara, K. Niita, A. Ohnishi, T. Sato, T. Song, A. Sorensen, N. Wang, W.-J. Xie, **Transport model comparison studies of intermediate-energy heavy-ion collisions**, Prog. Part. Nucl. Phys. 125 (2022) 103962. doi:<https://doi.org/10.1016/j.pnpnp.2022.103962>. URL <https://www.sciencedirect.com/science/article/pii/S0146641022007566>
- [26] R. Charity, M. McMahan, G. Wozniak, R. McDonald, L. Moretto, D. Sarantites, L. Sobotka, G. Guarino, A. Pantaleo, L. Fiore, A. Gobbi, K. Hildenbrand, **Systematics of complex fragment emission in niobium-induced reactions**, Nucl. Phys. A 483 (1988) 371–405. doi:[https://doi.org/10.1016/0375-9474\(88\)90542-8](https://doi.org/10.1016/0375-9474(88)90542-8). URL <https://www.sciencedirect.com/science/article/pii/0375947488>
- [27] J. Su, F.-S. Zhang, B.-A. Bian, **Odd-even effect in heavy-ion collisions at intermediate energies**, Phys. Rev. C 83 (2011) 014608. doi:<https://doi.org/10.1103/PhysRevC.83.014608>. URL <https://link.aps.org/doi/10.1103/PhysRevC.83.014608>
- [28] J. Sun, Z. H. Li, C. Guo, **Influence of the nuclear level density on the odd-even staggering in heavy-ion collisions**, Phys. Rev. C 97 (2018) 054604. doi:<https://doi.org/10.1103/PhysRevC.97.054604>. URL <https://link.aps.org/doi/10.1103/PhysRevC.97.054604>
- [29] J. Su, B.-H. Sun, S. Terashima, J.-W. Zhao, X.-D. Xu, J.-C. Zhang, G. Guo, L.-C. He, W.-P. Lin, W.-J. Lin, C.-Y. Liu, C.-G. Lu, B. Mei, Z.-Y. Sun, I. Tanihata, M. Wang, F. Wang, S.-T. Wang, X.-L. Wei, J. Wang, J.-Y. Xu, J.-R. Liu, M.-X. Zhang, Y. Zheng, L.-H. Zhu, X.-H. Zhang, **New measurement of the elemental fragmentation cross sections of 218 mev/nucleon**, Phys. Rev. C 107 (2023) 024609. doi:<https://doi.org/10.1103/PhysRevC.107.024609>. URL <https://link.aps.org/doi/10.1103/PhysRevC.107.024609>
- [30] C. Louchart, A. Obertelli, A. Boudard, F. Flavigny, **Nucleon removal from unstable nuclei investigated via intranuclear cascade**, Phys. Rev. C 83 (2011) 011601. doi:<https://doi.org/10.1103/PhysRevC.83.011601>. URL <https://link.aps.org/doi/10.1103/PhysRevC.83.011601>
- [31] J. Xia, W. Zhan, B. Wei, Y. Yuan, M. Song, W. Zhang, X. Yang, P. Yuan, D. Gao, H. Zhao, X. Yang, G. Xiao, K. Man, J. Dang, X. Cai, Y. Wang, J. Tang, W. Qiao, Y. Rao, Y. He, L. Mao, Z. Zhou, **The heavy ion cooler-storage-ring project (hirfl-csr) at lanzhou**, Nucl. Instrum. Methods Phys. Res., Sect. A 488 (2002) 11–25. doi:[https://doi.org/10.1016/S0168-9002\(02\)00475-8](https://doi.org/10.1016/S0168-9002(02)00475-8). URL <https://www.sciencedirect.com/science/article/pii/S0168900202004758>
- [32] W. Zhan, H. Xu, G. Xiao, J. Xia, H. Zhao, Y. Yuan, **Progress in hirfl-csr**, Nucl. Phys. A 834 (2010) 694c–700c. doi:<https://doi.org/10.1016/j.nuclphysa.2010.01.126>. URL <https://www.sciencedirect.com/science/article/pii/S037594741000126>
- [33] B.-H. Sun, J.-W. Zhao, X.-H. Zhang, L.-N. Sheng, Z.-Y. Sun, I. Tanihata, S. Terashima, Y. Zheng, L.-H. Zhu, L.-M. Duan, L.-C. He, R.-J. Hu, G.-S. Li, W.-J. Lin, W.-P. Lin, C.-Y. Liu, Z. Liu, C.-G. Lu, X.-W. Ma, L.-J. Mao, Y. Tian, F. Wang, M. Wang, S.-T. Wang, J.-W. Xia, X.-D. Xu, H.-S. Xu, Z.-G. Xu, J.-C. Yang, D.-Y. Yin, Y.-J. Yuan, W.-L. Zhan, Y.-H. Zhang, X.-H. Zhou, **Towards the full commissioning of the ribll2 beam line at the hirfl-csr complex**, Sci. Bull. 63 (2018) 78–80. doi:<https://doi.org/10.1016/j.scib.2017.12.014>. URL <https://www.sciencedirect.com/science/article/pii/S2095927318300614>
- [34] J.-W. Zhao, B.-H. Sun, L.-C. He, W.-P. Lin, C.-Y. Liu,

- I. Tanihata, S. Terashima, Y. Tian, F. Wang, M. Wang, G.-X. Zhang, X.-H. Zhang, L.-H. Zhu, L.-M. Duan, R.-J. Hu, Z. Liu, C.-G. Lu, P.-P. Ren, L.-N. Sheng, Z.-Y. Sun, S.-T. Wang, T.-F. Wang, Z.-G. Xu, Y. Zheng, Plastic scintillation detectors for precision time-of-flight measurements of relativistic heavy ions, *Chin. Phys. C* 41 (2017) 066001. doi:10.1088/1674-1137/41/6/066001. URL <https://dx.doi.org/10.1088/1674-1137/41/6/066001>
- [35] J. Zhao, B. Sun, L. He, G. Li, W. Lin, C. Liu, Z. Liu, C. Lu, D. Shen, Y. Sun, Z. Sun, I. Tanihata, S. Terashima, D. Tran, F. Wang, J. Wang, S. Wang, X. Wei, X. Xu, L. Zhu, J. Zhang, X. Zhang, Y. Zhang, Z. Zhou, Improvement of charge resolution for radioactive heavy ions at relativistic energies using a hybrid detection system, *Nucl. Instrum. Methods Phys. Res., Sect. A* 930 (2019) 95–99. doi:10.1016/j.nima.2019.03.063. URL <https://www.sciencedirect.com/science/article/pii/S0168900219300366>
- [36] G. A. Lalazassis, T. Nikšić, D. Vretenar, P. Ring, New relativistic mean-field interaction with density-dependent meson-nucleon couplings, *Phys. Rev. C* 71 (2005) 024312. doi:10.1103/PhysRevC.71.024312. URL <https://link.aps.org/doi/10.1103/PhysRevC.71.024312>
- [37] E. Chabanat, P. Bonche, P. Haensel, J. Meyer, R. Schaeffer, A skyrme parametrization from subnuclear to neutron star densities, *Nucl. Phys. A* 627 (1997) 710–746. doi:10.1016/S0375-9474(97)00596-4. URL <https://www.sciencedirect.com/science/article/pii/S0375947497005964>
- [38] W. Hauser, H. Feshbach, The inelastic scattering of neutrons, *Phys. Rev.* 87 (1952) 366–373. doi:10.1103/PhysRev.87.366. URL <https://link.aps.org/doi/10.1103/PhysRev.87.366>
- [39] W. Dilg, W. Schantl, H. Vonach, M. Uhl, Level density parameters for the back-shifted fermi gas model in the mass range 40 $A \leq 250$, *Nucl. Phys. A* 217 (1973) 269–298. doi:10.1016/0375-9474(73)90196-6. URL <https://www.sciencedirect.com/science/article/pii/S0375947473001966>
- [40] G. Audi, A. Wapstra, C. Thibault, The ame2003 atomic mass evaluation: (ii). tables, graphs and references, *Nucl. Phys. A* 729 (2003) 337–676. doi:10.1016/j.nuclphysa.2003.11.003. URL <https://www.sciencedirect.com/science/article/pii/S0375947403001008>
- [41] S. Yamaki, T. Yamaguchi, J. Kouno, K. Sato, N. Ichihashi, T. Suzuki, K. Abe, Y. Abe, M. Fukuda, H. Furuki, N. Inaba, K. Iwamoto, T. Izumikawa, Y. Kamisho, N. Kikuchi, A. Kitagawa, M. Mihara, S. Miyazawa, S. Momota, Y. Morita, D. Nagae, M. Nagashima, Y. Nakamura, R. Nishikiori, D. Nishimura, I. Nishizuka, T. Ohtsubo, J. Ohno, A. Ozawa, T. Sakai, S. Sato, D. Sera, F. Suzuki, S. Suzuki, S. Suzuki, M. Wakabayashi, M. Yaguchi, S. Yasumoto, Systematic study of individual charge-changing cross sections of intermediate-energy projectiles, *Nucl. Instrum. Methods Phys. Res., Sect. B* 317 (2013) 774–778. doi:10.1016/j.nimb.2013.05.057. URL <https://www.sciencedirect.com/science/article/pii/S0168583X13006387>
- [42] S.-Y. Jin, Y.-Z. Sun, S.-T. Wang, Z.-Y. Sun, X.-H. Zhang, Z.-Q. Chen, B. Mei, Y.-X. Zhao, S.-W. Tang, Y.-H. Yu, D. Yan, F. Fang, Y.-J. Zhang, S. bo Ma, X.-M. Liu, R. Han, Fragmentation of stable and neutron-rich 12-16c into boron fragments at approximately 40 MeV, *Chin. Phys. C* 46 (2022) 014003. doi:10.1088/1674-1137/ac2ed5. URL <https://dx.doi.org/10.1088/1674-1137/ac2ed5>
- [43] J. Su, W. Trautmann, L. Zhu, W.-J. Xie, F.-S. Zhang, Dynamical properties and secondary decay effects of projectile fragmentations in $^{12}\text{C} + ^{29}\text{Si}$ collisions, *Phys. Rev. C* 98 (2018) 014610. doi:10.1103/PhysRevC.98.014610. URL <https://link.aps.org/doi/10.1103/PhysRevC.98.014610>
- [44] J. Su, L. Zhu, E. Xiao, Fluctuations of the largest fragment charge in projectile fragmentation, *Phys. Rev. C* 105 (2022) 024608. doi:10.1103/PhysRevC.105.024608. URL <https://link.aps.org/doi/10.1103/PhysRevC.105.024608>
- [45] K. Sümmerer, Improved empirical parametrization of fragmentation cross sections, *Phys. Rev. C* 86 (2012) 014601. doi:10.1103/PhysRevC.86.014601. URL <https://link.aps.org/doi/10.1103/PhysRevC.86.014601>
- [46] X. Zhang, Modified epax2 parameterization for estimating the fragment cross sections of intermediate energy projectiles, *Nucl. Phys. A* 915 (2013) 59–69. doi:10.1016/j.nuclphysa.2013.06.013. URL <https://www.sciencedirect.com/science/article/pii/S0375947413006284>
- [47] B. Mei, Improved empirical parameterization for projectile fragmentation cross sections, *Phys. Rev. C* 95 (2017) 034608. doi:10.1103/PhysRevC.95.034608. URL <https://link.aps.org/doi/10.1103/PhysRevC.95.034608>
- [48] J.-J. Gaimard, K.-H. Schmidt, A reexamination of the abrasion-ablation model for the Nucl. Phys. A 531 (1991) 709–745. doi:10.1016/0375-9474(91)90748-U. URL <https://www.sciencedirect.com/science/article/pii/S0375947491000366>
- [49] J. Wilson, J. Shinn, L. Townsend, R. Tripathi, F. Badavi, S. Chun, Nucfrg2: A semiempirical nuclear fragmentation model, *Nucl. Instrum. Methods Phys. Res., Sect. B* 94 (1994) 95–102. doi:10.1016/0168-583X(94)95662-6. URL <https://www.sciencedirect.com/science/article/pii/S0168583X94000366>
- [50] G. Iancu, F. Flesch, W. Heinrich, Single fragmentation cross sections of 400amev 36ar and 40ar in collisions with lig, *Radiat. Meas.* 39 (2005) 525–533. doi:10.1016/j.radmeas.2004.10.011. URL <https://www.sciencedirect.com/science/article/pii/S1350448704003966>
- [51] C. Zeitlin, S. Guetersloh, L. Heilbronn, J. Miller, A. Fukumura, Y. Iwata, T. Murakami, L. Sihver, D. Mancusi, Fragmentation cross sections of medium-energy ^{35}Cl , ^{40}Ar , and ^{48}Ti beams on elements, *Phys. Rev. C* 77 (2008) 034605. doi:10.1103/PhysRevC.77.034605. URL <https://link.aps.org/doi/10.1103/PhysRevC.77.034605>
- [52] C. Zeitlin, L. Heilbronn, J. Miller, S. E. Rademacher, T. Borak, T. R. Carter, K. A. Frankel, W. Schimmerling, C. E. Stronach, Heavy fragment production cross sections from 1.05 gev/nucleon ^{56}Fe in c, al, cu, pb collisions, *Phys. Rev. C* 56 (1997) 388–397. doi:10.1103/PhysRevC.56.388. URL <https://link.aps.org/doi/10.1103/PhysRevC.56.388>
- [53] K. Sawahata, A. Ozawa, Y. Saito, Y. Abe, Y. Ichikawa, N. Inaba, Y. Ishibashi, A. Kitagawa, S. Matsunaga, T. Moriguchi, D. Nagae, S. Okada, S. Sato, S. Suzuki, T. Suzuki, Y. Takeuchi, T. Yamaguchi, J. Zenihiro, Investigations of charge-changing processes for light proton-rich nuclei on carbon and silicon, *Nucl. Phys. A* 961 (2017) 142–153. doi:10.1016/j.nuclphysa.2017.02.012. URL <https://www.sciencedirect.com/science/article/pii/S0375947417000968>
- [54] C. Zeitlin, A. Fukumura, S. Guetersloh, L. Heilbronn, Y. Iwata, J. Miller, T. Murakami, Fragmentation cross sections of ^{28}Si at beam energies from 290a to 1200a mev, *Nucl. Phys. A* 784 (2007) 341–367. doi:10.1016/j.nuclphysa.2006.10.088. URL <https://www.sciencedirect.com/science/article/pii/S0375947406010808>
- [55] M. Tanaka, M. Takechi, A. Homma, A. Prochazka, M. Fukuda, D. Nishimura, T. Suzuki, T. Moriguchi, D. S. Ahn, A. Aimaganbetov, M. Amano, H. Arakawa, S. Bagchi, K.-H. Behr, N. Burtebayev, K. Chikaato, H. Du, T. Fujii, N. Fukuda, H. Geissel, T. Hori, S. Hoshino, R. Igosawa, A. Ikeda, N. Inabe, K. Inomata, K. Kashi, Y. Kamikawa, D. Kamioka, N. Kanda, I. Kato, I. Kenzhina, Z. Korkulu, Y. Kuk, K. Kusaka, K. Matsuta, M. Mihara, E. Miyata, D. Nagae, S. Nakamura, M. Nassurulla, K. Nishimuro, T. Ohtsubo, K. Ohnishi, M. Ohtake, T. Ohtsubo, S. Omika, H. J. Ong, A. Ozawa, H. Sakurai, C. Scheidenberger, Y. Shimizu, T. Sugihara, T. Sumikama, H. Suzuki, S. Suzuki, H. Takeda, Y. Tanaka, Y. K. Tanaka, I. Tanihata, T. Wada, K. Wakayama, S. Yagi, T. Yamaguchi, R. Yamaguchi, Y. Yanagisawa, K. Yoshida, T. K. Zholdybayev, Charge-changing cross sections for $^{42-51}\text{Ca}$ and effect of charged-particle evaporation, *Phys. Rev. C* 106 (2022) 014617. doi:10.1103/PhysRevC.106.014617. URL <https://link.aps.org/doi/10.1103/PhysRevC.106.014617>
- [56] J. Zhao, B.-H. Sun, I. Tanihata, S. Terashima, A. Prochazka, J. Xu, L. Zhu, J. Meng, J. Su, K. Zhang, L. Geng, L. He, C. Liu, G. Li, C. Tian, W. Lin, W. Jia, Z. Ren, Z. Sun, F. Wang, J. Wang, M. Wang, S. Wang, X. Wei, X. Xu, J. Zhang, M. Zhang, X. Zhang, Isospin-dependence of the charge-changing cross-section shaped by the charged-particle evaporation, *Phys. Lett. B* 847 (2023) 138269. doi:10.1016/j.physletb.2023.138269. URL <https://www.sciencedirect.com/science/article/pii/S0370269323006284>
- [57] J. Zhang, B. Sun, I. Tanihata, R. Kanungo, C. Scheidenberger, S. Altmann, F. Ameal, J. Atkinson, Y. Ayyad, S. Bagchi, D. Cortina-Gil, I. Dillmann, A. Estradé, A. Evdokimov, F. Farinon, H. Geissel, G. Guastalla, R. Janik, S. Kaur, R. Knöbel, M. Krawczynski, Y. Litvinov, M. Marta, M. Mostazo, I. Mukha, G. Nociforo, H. J. Ong, S. Pietri, A. Prochazka, B. Sitar, P. Strmen, M. Takechi, J. Tanaka, J. Vargas, H. Weick, J. S. Winfield, A new approach for deducing rms proton radii from charge-changing reactions of neu

Sci. Bull. 69 (2024) 1647–1652. doi:<https://doi.org/10.1016/j.scib.2024.03.051>.
URL <https://www.sciencedirect.com/science/article/pii/S209592732400207X>